Physical Insights Into the Performances of Negative Capacitance Field Effect Transistors Using Single-Domain Versus Multidomain Models

Ming-Hao Li, Guan-You He, Qiang Li, Lei-Ying Ying, Bao-Ping Zhang, and Zhi-Wei Zheng, *Member, IEEE*

***Abstract*—In this study, the performances of negative capacitance field effect transistors (NCFETs) are compared by simulation using single-domain (SD) and multidomain (MD) models. Based on the MD model with the gradient energy coefficient, the ferroelectric (FE) polarization distribution is investigated. The results reveal the correlation among the FE polarization distribution, the NC effect, and the device performances for different device parameters, including the FE thickness (T_{FE}) and the oxide thickness (T_{OX}). The FE polarization distribution tends to transform from the SD state into the MD state with the increase of T_{FE} and the decrease of T_{OX}. The increased T_{FE} and decreased T_{OX} could result in a more significant distinction in the FE polarization distribution and a further larger difference in the NC effect between the MD state and the conventional SD state for NCFETs. The phenomenon above is confirmed by transient characteristics in NCFETs. More analysis and design space of NCFETs are provided by the study results.**

***Index Terms*—Ferroelectric (FE), multidomain (MD), negative capacitance, polarization switching.**

I. Introduction

NEGATIVE capacitance field effect transistors (NCFETs) have been considered a promising technology to reduce power consumption for next-generation transistors, due to gate voltage amplification by ferroelectric (FE) layer, providing the potential to overcome the physical limitation of 60 mV/dec for the subthreshold swing (SS) at room temperature. Numerous studies have explored the influence of device parameters on NCFETs in order to improve the device performances [1], [2], [3], [4], [5], [6], [7], [8], [9], [10], [11]. It has been proven that the use of an internal metal electrode between an FE and a dielectric will inherently destabilize NC due to FE domain formation [12]. The FE layer plays a key role in the improvement, and thus it is worth studying the polarization distribution of the FE layer. The previous research in NCFETs was mainly based on the conventional single-domain (SD) model without considering the gradient energy coefficient (k) [1], [2], [3], [4], [5], [6], [7], [8]. However, the polarization distribution for the NC effect was in relation to multidomain (MD) ferroelectricity [13], [14], which could be experimentally observed [15]. Recently, the related MD model without and with domain interaction has been proposed and applied in NC devices to investigate the FE polarization [12], [15], [16], [17], [18], [19], [20], [21], [22], [23], [24], [25], [26]. The effect of the device parameters, including the FE thickness (T_{FE}) and the oxide thickness (T_{OX}), on the FE polarization distribution has been studied in NC capacitors [20], [21], [22]. Moreover, the energy landscape of FE and the polarization–voltage (P–V) characteristics at different polarization states have been also studied in NC capacitors [24]. Nevertheless, there are only a few related reports in NCFETs [16], [18], [19], and the difference in transistor device performances between SD and MD states needs to be further investigated, since understanding the physical origin of the difference in NCFET performances between SD and MD states is very helpful for further research on NCFETs.

Therefore, in this study, we investigated the FE polarization switching in NCFETs with the MD model by considering k and evaluated the SD to MD transition with different device parameters by simulation. Moreover, the influence of such parameters on the FE polarization and the device performances was further analyzed to reveal the physical origin of the difference in device performances between SD and MD states. The results indicated that the polarization state of the FE region in NCFETs gradually changed from SD to MD state as the T_{FE} increased, the T_{OX} decreased or the gate voltage (V_g) increased. For the polarization distribution of the FE layer at the MD state, the domains became denser with the T_{FE} decreased and the maximum polarization intensity became smaller as the T_{OX} increased. The mechanism of the FE polarization switching was further analyzed. Based on this MD model and the conventional SD model, respectively, it was found that the difference of the SS became larger as the

Manuscript received 20 September 2022; revised 12 December 2022; accepted 19 December 2022. Date of publication 29 December 2022; date of current version 24 January 2023. The review of this article was arranged by Editor M. A. Pavanello. *(Corresponding author: Zhi-Wei Zheng.)*

The authors are with the School of Electronic Science and Engineering, Xiamen University, Xiamen 361005, China (e-mail: zwzheng@xmu.edu.cn).

Color versions of one or more figures in this article are available at https://doi.org/10.1109/TED.2022.3231227.

Digital Object Identifier 10.1109/TED.2022.3231227

T_{FE} increased and the T_{OX} decreased, which could be well explained by the FE polarization switching in MD-NCFETs. These present results could provide an experimental guideline for the design of future high-performance NCFETs.

II. Simulation Model and Principle

For the MD-based simulation, the MD model for the FE layer is established based on the Landau–Khalatnikov (LK) theory, which has been widely used in NC studies [1], [2], [3], [4], [5]. It can be given by [21]

$$\frac{1}{\Gamma}\frac{\mathrm{d}P}{\mathrm{d}t} + \nabla_P U_{\mathrm{FE}} = 0 \tag{1}$$

where Γ is the conductivity of polarization switching, P is the polarization, and U_{FE} is the total Gibb's free energy considering the Landau–Devonshire double-well energy landscape, stored electrostatic energy, and the free energy because of the polarization gradient at and around the domain wall (DW). The U_{FE} considering the MD state can be expressed as [24]

$$U_{\mathrm{FE}} = \alpha P^2 + \beta P^4 + \gamma P^6 + k(\nabla P)^2 - E_F P \tag{2}$$

where α, β, and γ are the FE anisotropy parameters, k is the coupling coefficient for the polarization gradient term of the free energy, E_F is the electric field obtained by the external voltage across the FE layer. Therefore, the MD-LK equation captured the effects of MD, and the resulting nonuniform polarization can be expressed as

$$-\frac{1}{\Gamma}\frac{\mathrm{d}P}{\mathrm{d}t} = 2\alpha P + 4\beta P^3 + 6\gamma P^5 - 2k\left(\frac{\mathrm{d}^2P}{\mathrm{d}x^2} + \frac{\mathrm{d}^2P}{\mathrm{d}z^2}\right) - E_F. \tag{3}$$

According to (3), the effect of the polarization variations in 2-D directions, including the x- and z-axis, is considered in our simulation. For this MD model, we assume that the polarization direction in the FE is in the upward (positive) or downward (negative) direction along the thickness of the film (z-axis), which is commonly set in the previously reported MD models [17], [18], [20], [21], [22]. In order to capture the FE polarization distribution and electrical characteristics of the NC devices, the Poisson equation, drift-diffusion equation, and the MD-LK equation mentioned above are solved simultaneously at every mesh point of the device. Table I shows the main simulation parameters for the NC devices based on the aforementioned MD model in this work. The corresponding parameters of the FE layer (HZO) are adopted from the previous reports [20], [22]. Here, the k value is an assumed value. And it is worth noting that the DW would be hard and the non-hysteretic NC effects would not be observed in HZO films if the k value is lower than a critical value [23].

Fig. 1(a) shows the schematic metal-ferroelectric-metal (MFM) and metal-ferroelectric-insulator-metal (MFIM) structures, respectively, which are commonly used for the NC effect study. Fig. 1(b) shows the simulated P–V characteristics of the FE in the MFM and MFIM capacitors, which could be obtained from the RC_{FE} simulation circuit diagram shown in the inset based on the parameters mentioned in Table I. The FE material passes through a region where the differential capacitance is negative when switching from one stable polarization to the other. By using the series resistor, the switching of the FE film is effectively slowed down to make it observable. Therefore, the NC transients can then be measured in RC_{FE} simulation circuit [27]. It was clearly observed that the P–V characteristic of the FE in the MFIM capacitor presented two windows at a certain voltage, which was different from that in the MFM capacitor. This phenomenon was also found in the previous reports [20], [21], [22]. Compared with the MFM capacitor, the charges of the MFIM capacitor induced by spontaneous polarization in the FE could not be compensated immediately due to the existence of the dead layer [24]. Therefore, the distribution of multiple domains with opposite polarization directions was a better choice to reduce the total energy, resulting in the MD state in the MFIM capacitor.

Fig. 2(a) illustrates the schematic structure and equivalent circuit of the NCFET device using HZO as the FE layer, in which the FE material parameters were consistent with those mentioned in Table I. Fig. 2(b) shows the I_d–V_g

TABLE I
MAIN SIMULATION PARAMETERS

Symbol	Quantity	Value
α		-1×10^{9} V·m/C
β	FE anisotropy parameters	-4×10^{8} V·m^5/C^3
γ		6×10^{10} V·m^9/C^5
k	gradient energy coefficient	1×10^{-11} V·m^3/C
Γ	conductivity of polarization switching	10 S/m
ϵ_{SiO_2}	relative dielectric constant for SiO_2	3.9
ϵ_{HZO}	relative dielectric constant for HZO	25
N_{sd}	S/D doping concentration (n^+)	10^{19} cm^{-3}
N_{ch}	channel doping concentration (p)	5×10^{17}cm^{-3}
L_g	gate length	100 nm

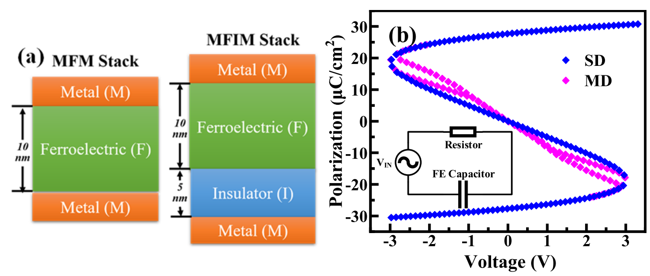

Fig. 1. (a) MFM and MFIM structures and (b) P–V characteristics of the FE in the MFM and MFIM capacitors with the inset of the RC_{FE} simulation circuit diagram.

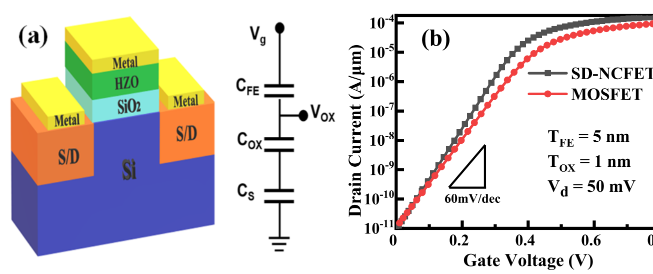

Fig. 2. (a) Schematic structure and equivalent circuit diagram of the NCFET device and (b) I_d–V_g characteristics of the SD-NCFET and baseline MOSFET.

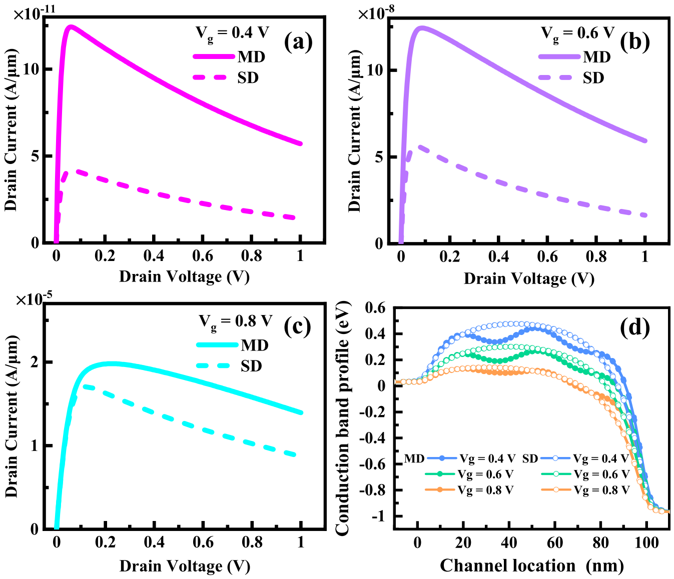

Fig. 3. I_d–V_d characteristics with $T_{\mathrm{FE}} = 10$ nm and $T_{\mathrm{OX}} = 3$ nm at (a) $V_g = 0.4$ V, (b) $V_g = 0.6$ V, (c) $V_g = 0.8$ V, and (d) conduction band profile at different V_g.

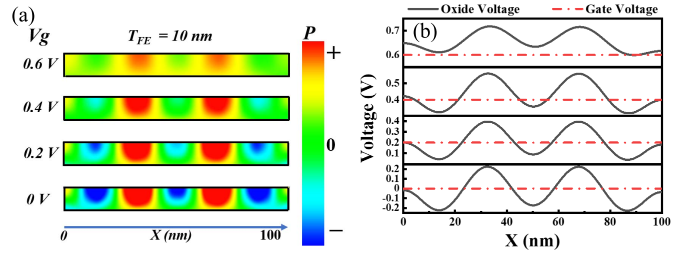

Fig. 4. (a) Dependency between the FE polarization distribution and V_g as $V_d = 0.05$ V. (b) Gate and oxide voltage distribution along the channel.

characteristics of the NCFET based on the conventional SD model (SD-NCFET) and the baseline MOSFET with the parameters shown in the inset and Table I. The obtained SS of the SD-NCFET and the baseline MOSFET were 56 and 66 mV/dec, respectively, resulting in the fact that the performances of the NCFET had achieved improvement due to the FE voltage amplification effect [7], [28], [29]. In this work, the FE polarization switching was simulated based on the MD model by considering k and the influence of the FE polarization switching on the device performances was subsequently investigated in comparison with the mentioned SD-NCFET.

III. Results and Discussion

Fig. 3(a)–(c) shows the output I_d–V_d characteristics of the NCFETs with different V_g based on the conventional SD and aforementioned MD models. It was clearly observed that the I_d decreased with the V_d increasing, which could be described as the negative differential resistance (NDR) effect. This NDR effect was caused due to the fringing field lines coupled to the channel region of the transistor. With increasing the drain bias, the fringing field lines coupled to the channel increased the potential barrier in the channel, resulting in the I_d reduction, which was different from the traditional MOSFET. Although the existence of NDR could lead to the hysteretic voltage transfer characteristics of the logic gates producing the higher noise margins, it could also compensate for the drain-induced barrier lowering (DIBL) effect in short channel MOSFET, pushing out the scalability limit of the CMOS devices [11]. As shown in Fig. 3(a)–(c), the NDR effect was more pronounced in the MD-NCFET as compared to the SD case. This phenomenon could be attributed to the different channel barriers affected by the FE polarization distribution in the SD and MD states, as shown in Fig. 3(d). The overall channel barrier in the SD state is higher than that in the MD state. Therefore, the FE polarization distribution in the MD state gives the device a larger I_d and generates a larger NDR effect. Moreover, it can be observed that the channel barriers in the SD and MD states became close as the V_g increased, resulting in the difference in the I_d–V_d curves between the SD and MD states becoming smaller and the overlap portion increased as the V_g increased. This could be also proved by the ratio of the maximum I_d at the MD state to that at the SD state, which exhibited a significantly decreasing trend with the increase of the V_g. The variation of the V_g caused a different influence on the output characteristics through the modification of the interface voltage by the FE polarization distribution as compared to the traditional MOSFETs. Therefore, the FE polarization distribution due to the variation of the V_g was of great importance and needed to be clarified.

Fig. 4(a) shows the variation of the polarization distribution in the FE layer along the channel with V_g when $T_{\mathrm{FE}} = 10$ nm and $T_{\mathrm{OX}} = 3$ nm in the MD-NCFET. It was clearly seen that the FE layer was in the MD state with existing both positive and negative polarization states at the same time. This polarization distribution seems symmetric, which is formed due to the FE to minimize the whole system energy. The formation of periodic alternating polarization contributes to the reduction of depolarization energy as well as free energy [30]. In addition, the V_d here was so small that it did not significantly affect the symmetry. As the V_g increased, the overall polarization intensity increased gradually, and the polarization distribution tended to be homogeneous. For NCFET operation, it was important to analyze the surface voltage of the oxide layer [denoted as the V_{OX} in Fig. 2(a)], which was related to the polarization distribution of the FE layer [22]. Fig. 4(b) shows the variation of the oxide voltage along the channel with V_g. It could be observed that the distribution of the V_g along the channel was uniform, while the distribution of the oxide voltage along the channel was not uniform. Moreover, with the V_g increasing, the oxide voltage along the channel also tended to be uniform, which was consistent with the trend of polarization distribution in Fig. 4(a). Note that the E_F distribution was opposite to the FE polarization distribution in the MD state. Therefore, the oxide voltage became nonhomogenous with the maximum and minimum values corresponding to the center of the domains with positive and negative polarization, respectively. As the V_g increased from 0 to 0.6 V, the difference between the maximum and min-

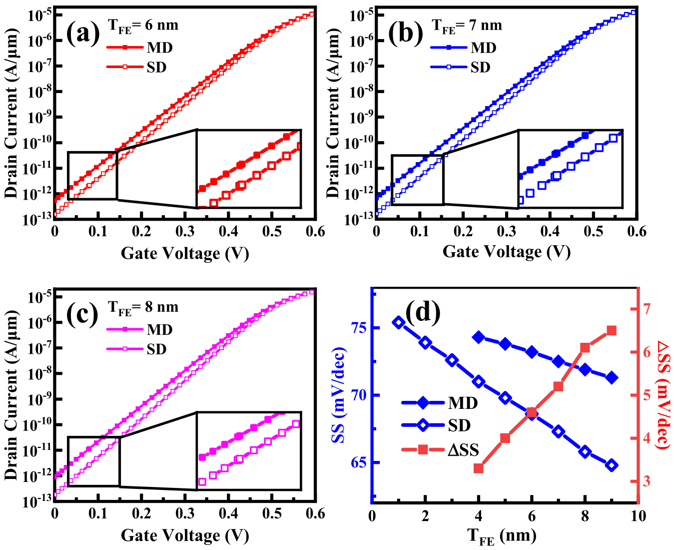

Fig. 5. I_d–V_g characteristics as V_d = 0.05 V with T_{OX} = 3 nm and (a) T_{FE} = 6 nm, (b) T_{FE} = 7 nm, (c) T_{FE} = 8 nm, and (d) extracted *SS* for different T_{FE} with T_{OX} = 3 nm based on the SD and MD models.

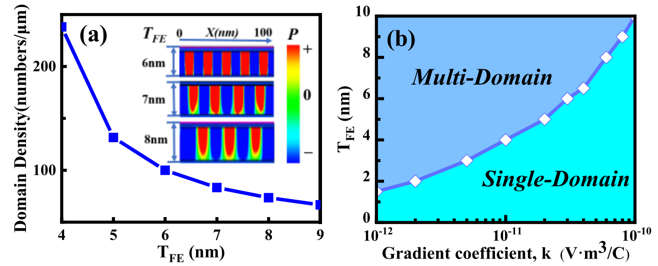

Fig. 6. (a) Relation between domain density and FE thickness with $k = 1 \times 10^{-11}$ V·m^3/C, and (b) conditions for SD and MD states for different k and T_{FE} with T_{OX} = 3 nm.

imum oxide voltage decreased from 0.4 to 0.1 V. This proved that the interface voltage was affected by the FE polarization distribution. Hence, the smaller difference in the I_d–V_d curves between the SD and MD states at larger V_g can be accounted for the tendency of the FE polarization distribution to change from MD to SD state as the V_g increased.

It was well known that the key factors including the T_{FE} and T_{OX} had a great impact on the NCFET performances based on the conventional SD model [7], [8], [9]. However, the MD formation due to the depolarization field, which was associated with the NC effect, could also play a key role in the NCFET performances. Consequently, we compared the I_d–V_g characteristics of the NCFETs with different T_{FE} based on the conventional SD and aforementioned MD models as shown in Fig. 5(a)–(c). Fig. 5(d) depicts the extracted SS for these devices. The SS decreased with the T_{FE} increasing for both the SD and MD states. The lower SS was obtained for the conventional SD model, indicating the better NC effect achieved in the SD state. Moreover, the difference in the SS (ΔSS) between the SD and MD states decreased with the T_{FE} decreasing, indicating that the NC effect in the MD state was closer to that in the SD state as the T_{FE} decreased.

To further explain the SS difference between the SD and MD models for different T_{FE}, the T_{FE} impact on the FE polarization distribution was investigated. Fig. 6(a) shows the relation between domain density and T_{FE} with fixed k. The domain density of the FE layer decreased as the T_{FE} increased. According to the Landau–Kittle formula [24], [30], for satisfying the minimum energy, the domain width (W) with an anti-parallel pattern in separate FE regions should be consistent with $W = (\sigma_\omega T_{FE}/1.7P^2)^{1/2}$ [30], which indicated that the W increased with the increase of the T_{FE}. Here, σ_ω was the DW energy density. Therefore, with the decrease in the T_{FE}, the domain pattern in the FE layer became denser. Fig. 6(b) shows the critical FE thickness of SD to MD transition (T_{SD-MD}) for NCFETs with various k at $V_g = 0$ V. It was observed that as the T_{FE} gradually increased, the FE polarization distribution changed from SD to MD state with fixed k. With the fixed $k = 1 \times 10^{-11}$ V·m^3/C, the FE polarization distribution changed from MD to SD state when $T_{FE} < 4$ nm, resulting in the SS of the MD curve in Fig. 5(d) starting from $T_{FE} = 4$ nm. The decrease of T_{FE} in the MD region was accompanied by the increase of the domain density as shown in Fig. 6(a), which makes the total energy of DW energy and depolarization energy increase. As the T_{FE} decreased into the SD region, the total energy of DW and depolarization energy was larger than the FE anisotropy energy, resulting in the SD state ($P = 0$). Moreover, the T_{SD-MD} gradually increased as the k increased. The k increase caused the increase in the DW energy and further in the total energy. Accordingly, the large T_{SD-MD} with high FE anisotropy energy was allowed to make FE stable in the SD state [22]. Therefore, the smaller difference in the SS between the SD and MD models with the smaller T_{FE} could be attributed to the enhancement of domain density, which was accompanied by the percentage of DW energy in the total energy improved as the T_{FE} scaled. Consequently, the MD state gradually transformed into the SD state with the reduction of the T_{FE}. The SS change of the devices was consistent with the change of the FE polarization distribution as the T_{FE} changed, indicating that the polarization state could affect the NC effect, which subsequently affected the device's performance.

Besides T_{FE}, the impact of the T_{OX} on the FE polarization distribution was also needed to be studied to select the appropriate value in the NCFET design. Fig. 7(a)–(c) shows the I_d–V_g characteristics of the NCFETs with different T_{OX} based on the conventional SD and aforementioned MD models, and Fig. 7(d) shows the extracted SS for these devices. As the T_{OX} decreased, the SS increased while the ΔSS decreased, indicating that the difference in the device performances between the SD and MD models became smaller. For further explanation, the T_{OX} impact on the FE polarization distribution was also investigated. Fig. 8(a) presents the change of FE polarization distribution for different T_{OX} with $T_{FE} = 5$ nm. It was observed that the FE polarization distribution tended to be suppressed and the maximum intensity of polarization decreased as the T_{OX} increased. The electric field in the depolarization field could be given by $E_{dep} = P[\varepsilon_0\varepsilon_{FE}(C_{OX}/C_{FE}+1)]^{-1}$ [31], where ε_0 and ε_{FE} were the vacuum and FE permittivity, respectively. The E_{dep} increased as the T_{OX} increased (C_{OX} decreased), resulting in suppressed polarization. Thus, the FE

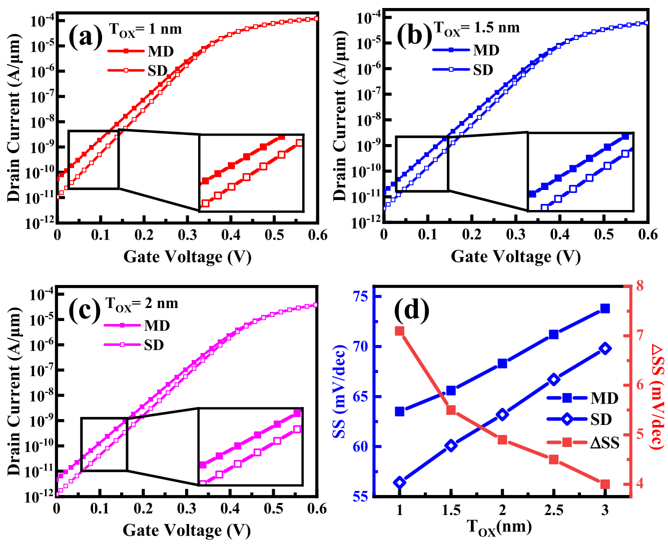

Fig. 7. I_d–V_g characteristics as V_d = 0.05 V with T_{FE} = 5 nm and (a) T_{OX} = 1 nm, (b) T_{OX} = 1.5 nm, (c) T_{OX} = 2 nm, and (d) extracted SS for different T_{OX} with T_{FE} = 5 nm based on the SD and MD models.

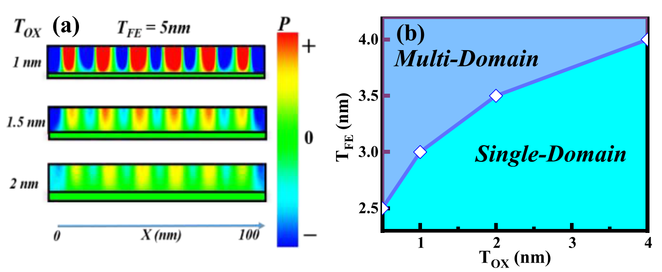

Fig. 8. (a) Dependency between the distribution of FE polarization and T_{OX}, and (b) conditions for MD states and SD states for different T_{OX} and T_{FE} with $k = 1 \times 10^{-11}$ V·m^3/C.

polarization distribution tended to be homogeneous and the FE state transformed from MD to SD with the T_{OX} increase as shown in Fig. 8(b). The FE anisotropy energy was constant as the T_{FE} was a certain value. The FE polarization distribution changed from MD to SD state as the T_{OX} increased, which could be explained by the increased total energy of the DW and depolarization energy with the T_{OX} increase. Since the larger T_{FE} had lower DW energy, depolarization energy, and higher FE anisotropy energy, it needed a larger T_{FE} to achieve the transition from the SD to MD state as the T_{OX} increased. Hence, the T_{SD-MD} gradually increased with the increased T_{OX}. Therefore, as the T_{OX} increased, the FE polarization was suppressed and the polarization distribution changed from MD to SD state, which made the NC effect in the MD state close to that in the SD state. It indicated that the T_{OX} had an impact on the FE polarization distribution as well as the NCFET performances.

IV. Conclusion

The performances of the NCFETs were compared by simulation using the conventional SD and aforementioned MD models in this study. The FE polarization distribution and the transition from the SD to MD state for the NCFETs were revealed. The results show that the device parameters including T_{FE} and T_{OX} could affect the FE polarization distribution, which could further affect the device performances by affecting the NC effect. The physical origin of the difference in the device performances based on the SD and MD models was analyzed by determining FE polarization distribution in NCFETs, which could provide a reference for the design and fabrication of future practical high-performance NCFETs.

References

[1] H. Agarwal et al., "Proposal for capacitance matching in negative capacitance field-effect transistors," *IEEE Electron Device Lett.*, vol. 40, no. 3, pp. 463–466, Mar. 2019, doi: 10.1109/LED.2019.2891540.

[2] G. Pahwa, A. Agarwal, and Y. S. Chauhan, "Numerical investigation of short-channel effects in negative capacitance MFIS and MFMIS transistors: Subthreshold behavior," *IEEE Trans. Electron Devices*, vol. 65, no. 11, pp. 5130–5136, Nov. 2018, doi: 10.1109/TED.2018.2870519.

[3] M.-Y. Kao et al., "Variation caused by spatial distribution of dielectric and ferroelectric grains in a negative capacitance field-effect transistor," *IEEE Trans. Electron Devices*, vol. 65, no. 10, pp. 4652–4658, Oct. 2018, doi: 10.1109/TED.2018.2864971.

[4] Y.-H. Liao, D. Kwon, Y.-K. Lin, A. J. Tan, C. Hu, and S. Salahuddin, "Anomalously beneficial gate-length scaling trend of negative capacitance transistors," *IEEE Electron Device Lett.*, vol. 40, no. 11, pp. 1860–1863, Nov. 2019, doi: 10.1109/LED.2019.2940715.

[5] H. Mehta and H. Kaur, "Impact of Gaussian doping profile and negative capacitance effect on double-gate junctionless transistors (DGJLTs)," *IEEE Trans. Electron Devices*, vol. 65, no. 7, pp. 2699–2706, Jul. 2018, doi: 10.1109/TED.2018.2832843.

[6] H. Mehta and H. Kaur, "Study on impact of parasitic capacitance on performance of graded channel negative capacitance SOI FET at high temperature," *IEEE Trans. Electron Devices*, vol. 66, no. 7, pp. 2904–2909, Jul. 2019, doi: 10.1109/TED.2019.2917775.

[7] H. Lee, Y. Yoon, and C. Shin, "Current-voltage model for negative capacitance field-effect transistors," *IEEE Electron Device Lett.*, vol. 38, no. 5, pp. 669–672, May 2017, doi: 10.1109/LED.2017.2679102.

[8] H. Agarwal et al., "NCFET design considering maximum interface electric field," *IEEE Electron Device Lett.*, vol. 39, no. 8, pp. 1254–1257, Aug. 2018, doi: 10.1109/LED.2018.2849508.

[9] Y. Choi, Y. Hong, and C. Shin, "Device design guideline for junctionless gate-all-around nanowire negative-capacitance FET with HfO_2-based ferroelectric gate stack," *Semicond. Sci. Technol.*, vol. 35, no. 1, Jan. 2020, Art. no. 015011, doi: 10.1088/1361-6641/ab5775.

[10] Y.-K. Lin et al., "Spacer engineering in negative capacitance FinFETs," *IEEE Electron Device Lett.*, vol. 40, no. 6, pp. 1009–1012, Jun. 2019, doi: 10.1109/LED.2019.2911104.

[11] J. Zhou et al., "Negative differential resistance in negative capacitance FETs," *IEEE Electron Device Lett.*, vol. 39, no. 4, pp. 622–625, Apr. 2018, doi: 10.1109/LED.2018.2810071.

[12] M. Hoffmann, M. Pesic, S. Slesazeck, U. Schroeder, T. Mikolajick, and T. Mikolajick, "Modeling and design considerations for negative capacitance field-effect transistors," in *Proc. Joint Int. EUROSOI Workshop Int. Conf. Ultimate Integr. Silicon (EUROSOI-ULIS)*, Apr. 2017, pp. 1–4, doi: 10.1109/ULIS.2017.7962577.

[13] A. M. Bratkovsky and A. P. Levanyuk, "Depolarizing field and 'real' hysteresis loops in nanometer-scale ferroelectric films," *Appl. Phys. Lett.*, vol. 89, no. 25, Dec. 2006, Art. no. 253108, doi: 10.1063/1.2408650.

[14] A. M. Bratkovsky and A. P. Levanyuk, "Very large dielectric response of thin ferroelectric films with the dead layers," *Phys. Rev. B, Condens. Matter*, vol. 63, no. 13, Apr. 2001, Art. no. 132103, doi: 10.1103/PhysRevB.63.132103.

[15] A. K. Yadav et al., "Spatially resolved steady-state negative capacitance," *Nature*, vol. 565, no. 7740, pp. 468–471, Jan. 2019, doi: 10.1038/s41586-018-0855-y.

[16] Y. Zhao et al., "Surface potential-based compact model for negative capacitance FETs compatible for logic circuit: With time dependence and multidomain interaction," in *IEDM Tech. Dig.*, San Francisco, CA, USA, Dec. 2019, pp. 7.5.1–7.5.4, doi: 10.1109/IEDM19573.2019.8993665.

[17] A. K. Saha, M. Si, K. Ni, S. Datta, P. D. Ye, and S. K. Gupta, "Ferroelectric thickness dependent domain interactions in FEFETs for memory and logic: A phase-field model based analysis," in *IEDM Tech. Dig.*, San Francisco, CA, USA, Dec. 2020, pp. 4.3.1–4.3.4, doi: 10.1109/IEDM13553.2020.9372099.

[18] A. K. Saha and S. K. Gupta, “Multidomain ferroelectric FETs with negative and enhanced positive capacitance for logic applications,” in *Proc. Int. Conf. Simul. Semiconductor Processes Devices (SISPAD)*, Sep. 2021, pp. 77–80, doi: 10.1109/SISPAD54002.2021.9592573.

[19] A. Cano and D. Jiménez, “Multidomain ferroelectricity as a limiting factor for voltage amplification in ferroelectric field-effect transistors,” *Appl. Phys. Lett.*, vol. 97, no. 13, Sep. 2010, Art. no. 133509, doi: 10.1063/1.3494533.

[20] P. Chang, G. Du, and X. Liu, “Design space for stabilized negative capacitance in HfO_2 ferroelectric-dielectric stacks based on phase field simulation,” *Sci. China Inf. Sci.*, vol. 64, no. 2, Feb. 2021, Art. no. 122402, doi: 10.1007/s11432-020-3005-8.

[21] H. W. Park, J. Roh, Y. B. Lee, and C. S. Hwang, “Modeling of negative capacitance in ferroelectric thin films,” *Adv. Mater.*, vol. 31, no. 32, Jun. 2019, Art. no. 1805266, doi: 10.1002/adma.201805266.

[22] A. K. Saha and S. K. Gupta, “Multidomain negative capacitance effects in metal-ferroelectric-insulator-semiconductor/metal stacks: A phase-field simulation based study,” *Sci. Rep.*, vol. 10, no. 1, Jun. 2020, Art. no. 10207, doi: 10.1038/s41598-020-66313-1.

[23] H.-J. Lee et al., “Scale-free ferroelectricity induced by flat phonon bands in HfO_2,” *Science*, vol. 369, no. 6509, pp. 1343–1347, Sep. 2020, doi: 10.1126/science.aba0067.

[24] A. K. Saha and S. K. Gupta, “Negative capacitance effects in ferroelectric heterostructures: A theoretical perspective,” *J. Appl. Phys.*, vol. 129, no. 8, Feb. 2021, Art. no. 080901, doi: 10.1063/5.0038971.

[25] K. J. Singh, A. Bulusu, and S. Dasgupta, “Multidomain negative capacitance effect in P(VDF-TrFE) ferroelectric capacitor and passive voltage amplification,” *IEEE Trans. Electron Devices*, vol. 67, no. 11, pp. 4696–4700, Nov. 2020, doi: 10.1109/TED.2020.3022745.

[26] D. Esseni and R. Fontanini, “Macroscopic and microscopic picture of negative capacitance operation in ferroelectric capacitors,” *Nanoscale*, vol. 13, no. 21, pp. 9641–9650, Jun. 2021, doi: 10.1039/d0nr06886a.

[27] M. Hoffmann et al., “Direct observation of negative capacitance in polycrystalline ferroelectric HfO_2,” *Adv. Funct. Mater.*, vol. 26, no. 47, pp. 8643–8649, Oct. 2016, doi: 10.1002/adfm.201602869.

[28] A. D. Gaidhane, G. Pahwa, A. Dasgupta, A. Verma, and Y. S. Chauhan, “Compact modeling of surface potential, drain current and terminal charges in negative capacitance nanosheet FET including quasi-ballistic transport,” *IEEE J. Electron Devices Soc.*, vol. 8, pp. 1168–1176, 2020, doi: 10.1109/JEDS.2020.3019927.

[29] C. Jin, T. Saraya, T. Hiramoto, and M. Kobayashi, “Physical mechanisms of reverse DIBL and NDR in FeFETs with steep subthreshold swing,” *IEEE J. Electron Devices Soc.*, vol. 8, pp. 429–434, 2020, doi: 10.1109/JEDS.2020.2986345.

[30] C. Kittel, “Theory of the structure of ferromagnetic domains in films and small particles,” *Phys. Rev.*, vol. 70, nos. 11–12, pp. 965–971, Dec. 1946, doi: 10.1103/PhysRev.70.965.

[31] J. Hoffman et al., “Ferroelectric field effect transistors for memory applications,” *Adv. Mater.*, vol. 22, nos. 26–27, pp. 2957–2961, Jul. 2010, doi: 10.1002/adma.200904327.